Dynamics of Human Head and Eye Rotations Under Donders' Constraint

Bijoy K. Ghosh, *Fellow, IEEE*, and Indika B. Wijayasinghe, *Member, IEEE*

***Abstract*—The rotation of human head and the eye are modeled as a perfect sphere with the rotation actuated by external torques. For the head movement, the axis of rotation is constrained by a law proposed in the 19th century by Donders. For the saccadic eye movement, Donders' Law is restricted to a law that goes by the name of Listing's Law. In this paper, head movement and saccadic eye movement are modeled using principles from classical mechanics and the associated Euler Lagrange's equations (EL) are analyzed. Geodesic curves are obtained in the space of allowed orientations for the head and the eye and projections of these curves on the space S^2 of pointing directions of the eye/head are shown. A potential function and a damping term has been added to the geodesic dynamics from EL and the resulting head and eye trajectories settle down smoothly towards the unique point of minimum potential. The minimum point can be altered to regulate the end point of the trajectories (potential control). Throughout the paper, the restricted dynamics of the eye and the head movement have been compared with the unrestricted rotational dynamics on SO(3) and the corresponding EL equations have been analyzed. A version of the Donders' Theorem, on the possible head orientations for a specific head direction, has been stated and proved in Appendix I. In the case of eye movement, Donders' Theorem restricts to the well known Listing's Theorem. In Appendix II, a constraint on the angular velocity and the angular acceleration vectors is derived for the head movement satisfying Donders' constraint. A statement of this constraint that goes by the name "half angle rule," has been derived.**

***Index Terms*—Donders' law, Euler Lagrange equation, eye/head movement, geodesics, half angle rule, Listing's Law, potential control, Riemannian Metric.**

I. Introduction

MODELING the dynamics of the eye and the head have been the research goals among neurologists, physiologists and engineers since 1845. Notable studies were conducted by Listing [1], Donders [2], and Helmholtz [3] and they claimed that the orientations of the eye and the head are completely determined as a function of the gaze and the heading directions, respectively. With the exception of occasional deviation, the eye follows what is known as the **Listing's Law** and likewise the head follows a generalization of the Listing's Law that goes by the name **Donders' Law**.

Eye movement and subsequently the head movement problem had found a renewed interest towards the later part of the 20th century [4]–[7]. Initially, the implementation of Listing's Law had been the primary focus of interest [8]–[13]. In spite of several notable modeling studies on three-dimensional eye and head movements (see [14]–[16] for a detailed review), there has not been a rigorous treatment of the three-dimensional head movement problem, in the framework of mechanical control system and classical mechanics [17]–[19]. In this paper, we continue to extend the approach of "geometric mechanics" presented in [20] to the dynamics of the head movement problems. Our motivation to study this problem is twofold. From the point of view of Biomechanics, we would like to understand how eye and head are controlled and coordinated while following the underlying Listing's and Donders' Laws. Our eventual goal is to focus on the combination of cost functions that are minimized while controlling gaze. Our second motivation is to control robotic head/eye (see Cannata [21]) that would follow these underlying principals. Understanding the principals of head/eye coordination would eventually help us build robotic head/eye that are humanlike.

Most of the earlier studies in eye movement have assumed that the head remained fixed and the eye is allowed to move freely. It has been observed by Listing (see [9]), that in this situation the orientation of the eye is completely determined by its gaze direction. Under Listing's constraint, starting from a frontal gaze, any other gaze direction is obtained by a rotation matrix whose axis of rotation is constrained to lie on a plane, called the Listing's Plane. Consequently, the set of all orientations the eye can assume is a submanifold of $\mathbf{SO}(3)$ (see Boothby [22] for a definition) called $\mathbf{LIST}$. Listing has shown that in a head fixed environment, eye orientations are restricted to this specific submanifold $\mathbf{LIST}$ (see [20] and [23]).

We study the dynamics, as the head moves spontaneously towards an object following a Listing like constraint that goes by the name Donders' constraint [4], [5] and [7]. Donders' law states that starting from a frontal head position, any other head orientation is obtained by a rotation matrix whose axis of rotation is constrained to lie on a two-dimensional surface, called the Donders' Surface [7]. Consequently, the set of all orientations the head can assume spontaneously is a submanifold of $\mathbf{SO}(3)$ called $\mathbf{DOND}$. Intuitively, Donders' surface is obtained by mildly perturbing the Listing's Plane along the torsional direction.

In a head free environment, the "axis of eye rotation" often jumps out of the Listing's plane during a saccade. We consider the "head free" case by introducing dynamics of eye-movement,

Manuscript received February 07, 2011; revised June 16, 2011; accepted September 26, 2011. Date of publication February 03, 2012; date of current version September 21, 2012. This work was supported in part by the National Science Foundation under Grant 0523983. Any opinions, findings, and conclusions or recommendations expressed in this material are those of the author(s) and do not necessarily reflect the views of the National Science Foundation. Recommended by Associate Editor Z. Qu.

The authors are with the Laboratory for BioCybernetics and Intelligent Systems, Texas Tech University, Lubbock, TX 79401 USA (e-mail: bijoy.ghosh@ttu.edu; indika.wijayasinghe@ttu.edu).

Color versions of one or more of the figures in this paper are available online at http://ieeexplore.ieee.org.

Digital Object Identifier 10.1109/TAC.2012.2186183

as shown in (1) at the bottom of the page, on the unconstrained orientation space $\mathbf{SO(3)}$. Even in this case, the orientation of the eye satisfies Listing's law, at the beginning and at the end point of a saccade.

The organization of this paper is as follows. In Section II, we introduce unit quaternions and motivate the operation of rotation using multiplication by unit quaternions (see [24] and [25]). In Section III, Donders' constraint is parameterized (following Tweed [12]) and we observe that Listing's constraint can be recovered as a special case of this parametrization. The spaces $\mathbf{LIST}$ and $\mathbf{DOND}$ are defined as a submanifold of $\mathbf{SO(3)}$. We state and prove **Listing's Theorem** which asserts that for all but one specific gaze direction (*viz.* the backward gaze direction), orientation of the eye is completely specified by the gaze direction. In Section IV, we introduce a Riemannian Metric for the associated spaces $\mathbf{LIST}$, $\mathbf{DOND}$ and $\mathbf{SO(3)}$ and write down the associated geodesic equations. In Section V, we define a Lagrangian using the Riemannian Metric in Section IV and a suitable Potential Energy term, and write down the corresponding Euler Lagrange Equations (EL). We also add an external "generalized torque" as inputs to the EL equations and this way we obtain a controlled dynamical system. In Section VI, we illustrate the obtained geodesic equations and the controlled dynamical system equations by a set of simulations. In these simulations, the control is either set to zero (see Fig. 4) or chosen to simulate an appropriate damping (see Figs. 5 and 6). The control system is regulated by an appropriate choice of a Potential Energy term. Finally Section VII concludes the paper. In Appendix I, we state and prove the **Donders' Theorem** for head movement which generalizes Listing's Theorem (see Section III) for eye movement. In Appendix II, we state and prove the half angle rule under Donders' constraint which generalizes the half angle rule for Listing's constraint. The half angle rule describes constraints on the angular velocity vectors and angular acceleration vectors, when the motion dynamics satisfy Listing's and Donders' laws.

II. Quaternionic Representations

Representation of "eye orientations" using the quaternions has already been described in [20]. Likewise, the head orientations can also be described using quaternions. In order to set up the notation, we revisit some of the main ideas in this section. A quaternion is a four tuple of real numbers denoted by Q. The space of unit quaternion is identified with the unit sphere in $\mathbf{R}^4$ and denoted by S^3. Each $q \in S^3$ can be written as

$$q = \cos\frac{\phi}{2}1 + \sin\frac{\phi}{2}n_1 i + \sin\frac{\phi}{2}n_2 j + \sin\frac{\phi}{2}n_3 k \qquad (2)$$

where $\phi \in [0, 2\pi]$, and $n = (n_1, n_2, n_3)$ is a unit vector in $\mathbf{R}^3$. If q is an unit quaternion represented as in (2), using simple properties of quaternion multiplication, one can show the following ([24], [25]):

"**The vector** $vec[q\bullet(v_1 i + v_2 j + v_3 k)\bullet q^{-1}]$ **is rotation of the vector** (v_1, v_2, v_3) **around the axis** n **by a counterclockwise angle** $\boldsymbol{\phi}$." The operator $vec[q]$ is defined to be the vector part of q and corresponds to the coefficients associated with i, j and k in (2).

To every unit quaternion in S^3, there corresponds a rotation matrix in $SO(3)$ (already introduced in [20]) and the correspondence is described by the map

$$rot : S^3 \to SO(3). \qquad (3)$$

Note that the map "rot" in (3) is surjective but not $1-1$. This is because both q and $-q$ in S^3 has the same image. We now write down a parametrization of the unit vector "n" in (2) as

$$n = (\cos\theta\ \cos\alpha\ \sin\theta\ \cos\alpha\ \sin\alpha). \qquad (4)$$

Combining (2) and (4), we have the following parametrization of unit quaternions:

$$q = \left(\cos\frac{\phi}{2}\ \sin\frac{\phi}{2}\cos\theta\cos\alpha\ \sin\frac{\phi}{2}\sin\theta\cos\alpha\ \sin\frac{\phi}{2}\sin\alpha\right). \qquad (5)$$

Using the coordinates (θ, ϕ, α) we have the following sequence of maps:

$$[0,\pi]\times[0,2\pi]\times\left[-\frac{\pi}{2},\frac{\pi}{2}\right] \xrightarrow{\rho} S^3 \xrightarrow{rot} SO(3) \xrightarrow{proj} S^2 \qquad (6)$$

where $\rho((\theta,\phi,\alpha)) = q$ (in (5)), $rot(q) = W$ and

$$proj(W) = \begin{pmatrix} \sin\theta\sin\phi\cos\alpha + \cos\theta\sin^2\frac{\phi}{2}\sin 2\alpha \\ -\cos\theta\sin\phi\cos\alpha + \sin\theta\sin^2\frac{\phi}{2}\sin 2\alpha \\ \cos^2\frac{\phi}{2} - \sin^2\frac{\phi}{2}\cos 2\alpha \end{pmatrix}. \qquad (7)$$

The matrix W in $SO(3)$ can be easily written from [20], and has been described in (1). The points in S^2 described by (7) provide a parameterization of the head (gaze) directions as a function of the coordinate angles θ, ϕ, α with respect to an initial head (gaze) direction of $(0,0,1)^T$, i.e., obtained by rotating the vector $(0,0,1)^T$ using the rotation matrix W.

III. Orientations Satisfying Donders' Constraint

Donders' law asserts that the axis of rotation "n" in (4) is restricted to a surface. We shall describe this surface by restricting

$$\alpha = \varepsilon\sin(2\theta) \qquad (8)$$

and obtain the axis of rotation as

$$n = (\cos\theta\cos(\varepsilon\sin(2\theta)), \sin\theta\cos(\varepsilon\sin(2\theta)), \sin(\varepsilon\sin(2\theta)))^T. \qquad (9)$$

$$\begin{pmatrix} \cos^2\frac{\phi}{2} - \sin^2\frac{\phi}{2}(1 - 2\cos^2\alpha\cos^2\theta) & \sin^2\frac{\phi}{2}\cos^2\alpha\sin(2\theta) - \sin\phi\sin\alpha & \sin^2\frac{\phi}{2}\sin(2\alpha)\cos\theta + \sin\phi\cos\alpha\sin\theta \\ \sin^2\frac{\phi}{2}\cos^2\alpha\sin(2\theta) + \sin\phi\sin\alpha & \cos^2\frac{\phi}{2} - \sin^2\frac{\phi}{2}(1 - 2\cos^2\alpha\sin^2\theta) & \sin^2\frac{\phi}{2}\sin(2\alpha)\sin\theta - \sin\phi\cos\alpha\cos\theta \\ \sin^2\frac{\phi}{2}\sin(2\alpha)\cos\theta - \sin\phi\cos\alpha\sin\theta & \sin^2\frac{\phi}{2}\sin(2\alpha)\sin\theta + \sin\phi\cos\alpha\cos\theta & \cos^2\frac{\phi}{2} - \sin^2\frac{\phi}{2}\cos(2\alpha) \end{pmatrix} \qquad (1)$$

The parameter ϵ is assumed to be a small positive or negative constant. The choice of (8) as a description of the Donders' surface is dictated by the following observation made in [12] about head movement.

> When the axis of rotation is horizontal or vertical (i.e., when θ is a multiple of $\pi/2$), head moves without any torsion. At other angles of rotation, there is a gradual increase in torsion.

Note that the axis of rotation vector n lies on a surface given by

$$2\varepsilon xy = \sin^{-1} z(1-z^2) \tag{10}$$

where (x, y, z) are the three coordinates of the axis of rotation given by $x = \cos\theta\cos\alpha$, $y = \sin\theta\cos\alpha$, $z = \sin\alpha$. The coordinate z is constrained by $|z| \leq |\sin\epsilon|$.

The Donders' law (8) constrains the rotation matrices W parameterized in (1). We define $\mathbf{DOND}$ to be the associated submanifold of $\mathbf{S}^3$ and $\mathbf{SO}_D(3)$ to be the associated submanifold of $\mathbf{SO(3)}$. They are both two-dimensional submanifolds parameterizing all possible rotations in $\mathbf{S}^3$ and $\mathbf{SO}(3)$, respectively, that satisfy Donders' constraint (8). The heading direction $(0,0,1)^T$ is transformed to the direction

$$\begin{pmatrix} \sin\theta\sin\phi\cos(\varepsilon\sin(2\theta)) + \cos\theta\sin^2\frac{\phi}{2}\sin(2\varepsilon\sin(2\theta)) \\ -\cos\theta\sin\phi\cos(\varepsilon\sin(2\theta)) + \sin\theta\sin^2\frac{\phi}{2}\sin(2\varepsilon\sin(2\theta)) \\ \cos^2\frac{\phi}{2} - \sin^2\frac{\phi}{2}\cos(2\varepsilon\sin(2\theta)) \end{pmatrix}$$

by the rotation matrix (1). Thus, we obtain from (6) the following sequence of maps:

$$[0,2\pi]\times[0,2\pi] \xrightarrow{\rho} \mathbf{DOND} \xrightarrow{rot} \mathbf{SO}_D(3) \xrightarrow{proj} \mathbf{S}^2 \tag{11}$$

where α has been restricted by the Donders' constraint (8). Note that the variable θ in (11) is restricted to the interval $[0,2\pi]$, whereas in (6) it is restricted to $[0,\pi]$. This is because the images of (θ,ϕ,α) and $(\theta+\pi,-\phi,-\alpha)$ are the same under the map ρ in (6). Hence, the domain of θ is chosen to be $[0,\pi]$ in (6). The points (θ,ϕ,α) and $(\theta+\pi,-\phi,-\alpha)$ cannot both satisfy the Donders' constraint unless $\epsilon = 0$. Hence, in (11) the domain has to be enlarged.

Listing's constraint is recovered from Donders' constraint by restricting ϵ to zero. Listing's law asserts that the axis of rotation "n" defined in (4), is restricted to a plane, called the Listing's Plane. We shall describe this plane by restricting $\alpha = 0$ and obtain $n = (\cos\theta, \sin\theta, 0)^T$, $q = (\cos(\phi/2), \sin(\phi/2)\cos\theta, \sin(\phi/2)\sin\theta, 0)^T$ and the matrix W can be obtained from (1). Analogous to the Donders' constraint, under the Listing's constraint, we define $\mathbf{LIST}$ to be the associated submanifold of $\mathbf{S}^3$ and $\mathbf{SO}_L(3)$ to be the associated submanifold of $\mathbf{SO(3)}$. We have the following sequence of maps:

$$[0,\pi]\times[0,2\pi] \xrightarrow{\rho} \mathbf{LIST} \xrightarrow{rot} \mathbf{SO}_L(3) \xrightarrow{proj} \mathbf{S}^2 \tag{12}$$

and the following theorem due to Listing.

Theorem 1 (Listing): Under the Listing's constraint, the map

$$\mathbf{SO}_L(3) - \left\{ \begin{pmatrix} \cos 2\theta & \sin 2\theta & 0 \\ \sin 2\theta & -\cos 2\theta & 0 \\ 0 & 0 & -1 \end{pmatrix} \right\} \xrightarrow{\mathbf{proj}} \mathbf{S}^2 - \left\{ \begin{pmatrix} 0 \\ 0 \\ -1 \end{pmatrix} \right\}$$

described by (6) and (12) is one to one and onto.

Remark: Listing's Theorem 1 asserts that for all but perhaps one gaze direction given by $(0,0,-1)^T$, which is opposite to the primary gaze direction $(0,0,1)^T$, every other gaze direction completely specifies the rotation matrix.

Proof of Listing's Theorem 1: Note that when $\phi \neq 0$ and $\phi \neq \pi$, it follows that if $\theta = \theta_0, \phi = \phi_0$ satisfies a suitable gaze direction, then $\theta = \theta_0 + \pi, \phi = 2\pi - \phi_0$ would also satisfy the same gaze direction. In the domain $\theta \in [0,\pi]$ and $\phi \in [0,2\pi]$ these are the only two choices for a specific gaze vector. It would follow that when $\phi \neq 0$, $\phi \neq \pi$, $\theta \neq 0$ and $\theta \neq \pi$ then the pair of angles θ, ϕ in the domain that satisfies a suitable gaze direction is unique. Hence, these gaze directions correspond to an unique rotation matrix. It can be checked by direct calculations that for the pair $(\theta = 0, \phi = \phi_0)$ and $(\theta = \pi, \phi = -\phi_0)$ the corresponding rotation matrix and the gaze vector are identical. Finally for $\phi = 0$ or $\phi = 2\pi$, and θ is arbitrary, the rotation matrix is the identity matrix and the gaze direction is the primary gaze direction $(0,0,1)^T$. It would follow that the only gaze direction for which the rotation matrix is not unique is when $\phi = \pi$. This would correspond to the gaze direction $(0,0,-1)^T$, which has been excluded. $(\mathbf{Q.E.D})$

Remark: In Appendix I, we state and prove a generalization of the Listing's Theorem 1, for the head movement problem. We call this theorem the Donders' Theorem. The upshot of the theorem is that the number of orientations of the head for a specific pointing direction is "not unique" when the head follows the Donders' Law. For most practical pointing directions of the head, which includes the frontal hemisphere, the number of allowed orientations is two (counting multiplicity). For a simply connected, closed and bounded set $\mathbf{S}$ of head directions around the "backward direction" the number of orientations is four (counting multiplicity). When the parameter ϵ, in (8) approaches zero, the set $\mathbf{S}$ degenerates to a point, *viz.* the backward head direction and we recover the Listing's Theorem from Donders' Theorem. For a specific pointing direction in the frontal hemisphere, the two ambiguous head orientations merge to an unique orientation when ϵ approaches zero. The relative sizes of $\mathbf{S}$ as a function of ϵ has been illustrated in Fig. 9.

IV. Riemannian Metric on SO(3), DOND and LIST

It has been described in [20] that eye rotations are typically confined to a sub manifold $\mathbf{LIST}$ of $\mathbf{SO}(3)$ especially when the head is restrained to be fixed. Likewise, spontaneous head movements are typically confined to a sub manifold $\mathbf{DOND}$ of $\mathbf{SO}(3)$. In order to write down the equations of motion, one needs to know the kinetic and the potential energies of the head in motion. The kinetic energy is given by the induced Riemannian metric on $\mathbf{DOND}$, induced from the Riemannian metric on $\mathbf{SO}(3)$.

The Riemannian metric (see [26]) is derived by assuming that the head is a perfect sphere and its inertia tensor is equal to the identity matrix $I_{3\times 3}$. This is associated with a left invariant Riemannian metric on $\mathbf{SO}(3)$, already described in [20]. An easy way to carry out computation using this Riemannian metric is provided by the isometric submersion $\mathbf{rot}$ described in (3) and (6). In order to compute the Riemannian Metric on $\mathbf{SO}(3)$, we write

$$\rho_*\left(\frac{\partial}{\partial\theta}\right)=\begin{pmatrix}0\\ -\sin(\phi/2)\,\sin(\theta)\,\cos(\alpha)\\ \sin(\phi/2)\,\cos(\theta)\,\cos(\alpha)\\ 0\end{pmatrix}$$

$$\rho_*\left(\frac{\partial}{\partial\alpha}\right)=\begin{pmatrix}0\\ -\sin(\phi/2)\,\cos(\theta)\,\sin(\alpha)\\ -\sin(\phi/2)\,\sin(\theta)\,\sin(\alpha)\\ \sin(\phi/2)\,\cos(\alpha)\end{pmatrix}$$

$$\rho_*\left(\frac{\partial}{\partial\phi}\right)=\begin{pmatrix}-\frac{1}{2}\sin(\phi/2)\\ \frac{1}{2}\cos(\phi/2)\,\cos(\theta)\,\cos(\alpha)\\ \frac{1}{2}\cos(\phi/2)\,\sin(\theta)\,\cos(\alpha)\\ \frac{1}{2}\cos(\phi/2)\,\sin(\alpha)\end{pmatrix}.$$

Then we obtain the inner products given by

$$g_{11}=\left\langle\frac{\partial}{\partial\theta},\frac{\partial}{\partial\theta}\right\rangle=\sin^2(\phi/2)\cos^2(\alpha)$$
$$g_{22}=\left\langle\frac{\partial}{\partial\alpha},\frac{\partial}{\partial\alpha}\right\rangle=\sin^2(\phi/2)$$
$$g_{33}=\left\langle\frac{\partial}{\partial\phi},\frac{\partial}{\partial\phi}\right\rangle=\frac{1}{4}$$
$$\text{and } g_{ij}=0 \text{ for } i\neq j \text{ with } i,j=1,2,3.$$

The Riemannian metric on $\mathbf{SO}(3)$ is given by

$$g=\sin^2(\phi/2)\cos^2(\alpha)d\theta^2+\sin^2(\phi/2)d\alpha^2+\frac{1}{4}d\phi^2. \quad (13)$$

Note that restricted to the Donders' surface, i.e., when (8) is satisfied, the Riemannian metric on $\mathbf{DOND}$ is given by

$$g=\sin^2(\phi/2)\left[\cos^2\alpha+\left(\frac{\partial\alpha}{\partial\theta}\right)^2\right]d\theta^2+\frac{1}{4}d\phi^2. \quad (14)$$

Using the Riemannian metric (13) for $\mathbf{SO}(3)$, the associated geodesic equation is given by

$$\begin{aligned}\ddot{\theta}+\dot{\theta}\dot{\phi}\cot(\phi/2)-2\dot{\theta}\dot{\alpha}\tan(\alpha)&=0\\ \ddot{\phi}-(\dot{\theta})^2\sin(\phi)\cos^2(\alpha)-(\dot{\alpha})^2\sin(\phi)&=0\\ \ddot{\alpha}+\frac{1}{2}(\dot{\theta})^2\sin(2\alpha)+\dot{\phi}\dot{\alpha}\cot(\phi/2)&=0. \quad (15)\end{aligned}$$

Likewise, using the Riemannian metric (14) for $\mathbf{DOND}$, the associated geodesic equation is given by

$$\begin{aligned}&\frac{d}{dt}\left[\sin^2\frac{\phi}{2}\left(\cos^2\alpha+\left(\frac{\partial\alpha}{\partial\theta}\right)^2\right)\dot{\theta}\right]\\ &-\sin^2\frac{\phi}{2}\dot{\theta}^2\frac{\partial\alpha}{\partial\theta}\left[\frac{\partial^2\alpha}{\partial\theta^2}-\frac{1}{2}\sin(2\alpha)\right]=0\\ &\ddot{\phi}-\left[\cos^2\alpha+\left(\frac{\partial\alpha}{\partial\theta}\right)^2\right]\dot{\theta}^2\sin\phi=0. \quad (16)\end{aligned}$$

Restricted to the Listing's plane, i.e., when $\alpha=0$, the Riemannian metric on $\mathbf{LIST}$ is given by

$$g=\sin^2(\phi/2)d\theta^2+\frac{1}{4}d\phi^2 \quad (17)$$

and (15) reduces to the following pair of equations, already described in [20], given by

$$\ddot{\theta}+\dot{\theta}\dot{\phi}\cot(\phi/2)=0,\quad \ddot{\phi}-(\dot{\theta})^2\sin(\phi)=0. \quad (18)$$

We now state the following theorem, which demonstrates the geometric structure of the geodesic.

Theorem 2 (Geodesic curves on $\mathbf{SO(3)}$ and $\mathbf{SO}_L(3)$): The geodesic curves on $\mathbf{SO}(3)$, given by the integral curves of (15), projected on $\mathbf{S}^2$ via the mapping "proj" described in (6) are circles. Furthermore, the geodesic curves on $\mathbf{SO}_L(3)$, given by the integral curves of (18), projected on $\mathbf{S}^2$ via the mapping "proj" described in (12) are circles which always pass through a fixed vector $(0,0,-1)^T$.

Proof of the Geodesic Theorem 2: If we define a new angle variable

$$\xi=\frac{\phi}{2}$$

the parametrization of $\mathbf{S}^3$ described in (5) would be given by

$$q=(\cos\xi,\sin\xi\cos\theta\cos\alpha,\sin\xi\sin\theta\cos\alpha,\sin\xi\sin\alpha). \quad (19)$$

Using the angle variables (ξ,θ,α), it is easy to see using the Riemannian metric (13) on $\mathbf{S}^3$, that the geodesics are great circles on $\mathbf{S}^3$. What we need to show is that, under the composition map "proj $\circ$ rot," described by

$$\begin{pmatrix}\delta_0\\ \delta_1\\ \delta_2\\ \delta_3\end{pmatrix}\longmapsto\begin{pmatrix}2(\delta_1\delta_3+\delta_0\delta_2)\\ 2(\delta_2\delta_3-\delta_0\delta_1)\\ \delta_0^2+\delta_3^2-\delta_1^2-\delta_2^2\end{pmatrix}$$

"generically the great circles on $\mathbf{S}^3$ are projected as circles on $\mathbf{S}^2$." We omit the details of the proof but the essential point is that the great circles on $\mathbf{S}^3$ project as planar curves on $\mathbf{S}^2$ and hence generically they are circles (unless the circle degenerates to a point). When the Listing's constraint is satisfied, we have $\alpha=0$. The parametrization (19) would reduce to

$$q=(\cos\xi,\ \sin\xi\cos\theta,\ \sin\xi\sin\theta,\ 0).$$

It would follow that great circles on $\mathbf{S}^3$ are in fact great circles on $\mathbf{S}^2$, where $\mathbf{S}^2$ is parameterized as

$$(\cos\xi,\ \sin\xi\cos\theta,\ \sin\xi\sin\theta).$$

Since, every great circle on $\mathbf{S}^2$ passes through the point $\xi=\pi/2$, the circle on the gaze space $\mathbf{S}^2$ passes through the point $\phi=\pi$. The gaze corresponding to the point $\phi=\pi$ is precisely $(0,0,-1)$. $(\mathbf{Q.E.D})$

Remark: If we make the convention that the gaze direction vector $(0,0,1)^T$ is the frontal gaze direction, it would follow that the vector $(0,0,-1)^T$ is the backward gaze direction. Listing's Theorem 1 would then assert that for all gazes other than the backward gaze, orientation of the eye, restricted to the

Listing's submanifold of $\mathbf{SO}(3)$, is completely specified by the gaze. It may be inferred from the above geodesic Theorem 2 that the projections of the geodesic curves on the gaze space, $\mathbf{S}^2$, are circles that always pass through the backward gaze direction.

Remark: Geodesic curves on $\mathbf{SO}_D(3)$ are in general not periodic and does not appear to have a regular geometric shape. When the initial condition on $\dot{\theta}$ is assumed to be 0, the projection of the integral curves of (16) on $\mathbf{S}^2$ are circles (shown in Fig. 3). Interestingly, these circles always pass through the frontal pointing direction.

V. General Equation of Motion on SO(3) and Its Two Submanifolds

The Riemannian Metric that we have obtained in (14) enables us to write down an expression for the kinetic energy KE given by

$$KE = \frac{1}{2}\left[\sin^2(\phi/2)\left[\cos^2\alpha + \left(\frac{\partial\alpha}{\partial\theta}\right)^2\right]\dot{\theta}^2 + \frac{1}{4}\dot{\phi}^2\right]. \quad (20)$$

Remark: In writing the expression (20) for kinetic energy, we need to assume that the moment of inertia matrix is an identity matrix, as would be the case if the eye/head is a perfect sphere and all rotations are about its center.

In general, the dynamics is affected by an additional potential energy and an external input torque. Let us consider a general form of the potential function given by

$$V(\theta,\phi) = A\sin^2\frac{\phi-\phi_0}{2} + B\sin^2\frac{\theta-\theta_0}{2} \quad (21)$$

which attains a minimum value at a specific pointing direction (θ_0,ϕ_0).

Remark: Human eye and head orientations have a natural domain and they are not allowed to move outside this domain. In an uncontrolled system, one way to implement this would be to include a potential term V to the Lagrangian, with the property that the potential function is large at points that are disallowed. Our choice of the term (21) is arbitrary, except that it vanishes at (θ_0,ϕ_0) and takes large values when the eye and the head are pointed backwards. An interesting question that we have not answered in this paper is "Does there exist a potential function that would match observed human eye and head movements?"

The expression for the Lagrangian is given by $L = KE - V$, and the equation of motion is described by

$$\frac{d}{dt}\left(\frac{\partial L}{\partial\dot{\beta}}\right) - \left(\frac{\partial L}{\partial\beta}\right) = \tau_\beta$$

where β is the angle variable. Assuming $\phi_0 = \theta_0 = 0$ in (21), the Euler Lagrange's equation on $\mathbf{DOND}$ is given by

$$\frac{d}{dt}\left[\sin^2\frac{\phi}{2}\left(\cos^2\alpha + \left(\frac{\partial\alpha}{\partial\theta}\right)^2\right)\dot{\theta}\right]$$
$$-\sin^2\frac{\phi}{2}\dot{\theta}^2\frac{\partial\alpha}{\partial\theta}\left[\frac{\partial^2\alpha}{\partial\theta^2} - \frac{1}{2}\sin(2\alpha)\right] = -\frac{1}{2}B\sin\theta + \tau_\theta,$$
$$\ddot{\phi} - \left[\cos^2\alpha + \left(\frac{\partial\alpha}{\partial\theta}\right)^2\right]\dot{\theta}^2\sin\phi = -2A\sin\phi + 4\tau_\phi$$

where, as in Section III, we continue to assume that α satisfies the Donders' constraint (8). In order to describe (22) in a compact notation, we define the following set of variables:

$$\alpha(\theta) = \varepsilon\sin(2\theta), \quad \nu(\theta) = \varepsilon\cos(2\theta),$$
$$\sigma(\theta,\phi) = \sin^2\frac{\phi}{2}\left[\cos^2\alpha + 4\nu^2\right]. \quad (22)$$

We also define

$$\Lambda(\theta) = \frac{\nu\left(8\alpha + \sin(2\alpha)\right)}{\cos^2\alpha + 4\nu^2}$$

and rewrite (22) as follows:

$$\ddot{\theta} = -\frac{\dot{\sigma}}{\sigma}\dot{\theta} - \Lambda(\theta)\dot{\theta}^2 - \frac{B}{2\sigma}\sin\theta + \frac{1}{\sigma}\tau_\theta$$
$$\ddot{\phi} = (\cos^2\alpha + 4\nu^2)\sin\phi\dot{\theta}^2 - 2A\sin\phi + 4\tau_\phi \quad (23)$$

where

$$\dot{\sigma} = \frac{d}{dt}\left[\sigma(\theta,\phi)\right].$$

In order to write (23) using state variables, we write

$$z_1 = \theta, \quad z_2 = \dot{\theta}, \quad z_3 = \phi, \quad z_4 = \dot{\phi}$$

and the corresponding state variable equation on $\mathbf{DOND}$ is given by

$$\dot{z}_1 = z_2$$
$$\dot{z}_2 = -\frac{\dot{\sigma}}{\sigma}z_2 - \Lambda(z_1)z_2^2 - \frac{B}{2\sigma}\sin(z_1) + \frac{1}{\sigma}\tau_\theta$$
$$\dot{z}_3 = z_4$$
$$\dot{z}_4 = (\cos^2\alpha + 4\nu^2)(\sin z_3)z_2^2 - 2A\sin(z_3) + 4\tau_\phi \quad (24)$$

where $\alpha(z_1)$, $\nu(z_1)$, and $\sigma(z_1,z_3)$ can be defined from (22) and where the details of $\dot{\sigma}$ has been omitted.

Remark: The underlying control system that governs head movement satisfying Donder's constraint is given by (24). τ_θ and τ_ϕ are generalized torques that are generated by neck muscle forces acting on the head. For the eye movement problem, muscle forces generating these torques were modeled in [20]. For the head movement problem, modeling the muscle generated forces of the neck muscles, is a subject of future research.

The state variable equation on $\mathbf{LIST}$ can be obtained by considering $\alpha = 0$ and the Riemannian Metric given by (17). Assuming $\phi_0 = \theta_0 = 0$ in (21), the Euler Lagrange's Equation on $\mathbf{LIST}$ is given by

$$\ddot{\theta} + \dot{\theta}\dot{\phi}\cot(\phi/2) + \frac{B}{2}\csc^2(\phi/2)\sin(\theta) = \csc^2(\phi/2)\tau_\theta$$
$$\ddot{\phi} - (\dot{\theta})^2\sin(\phi) + 2\mathrm{A}\sin(\phi) = 4\tau_\phi. \quad (25)$$

The state variable equation on $\mathbf{SO(3)}$ can be obtained by considering the Riemannian Metric given by (13). These have not been written down in this paper, since we do not study control of motion dynamics on $\mathbf{SO(3)}$.

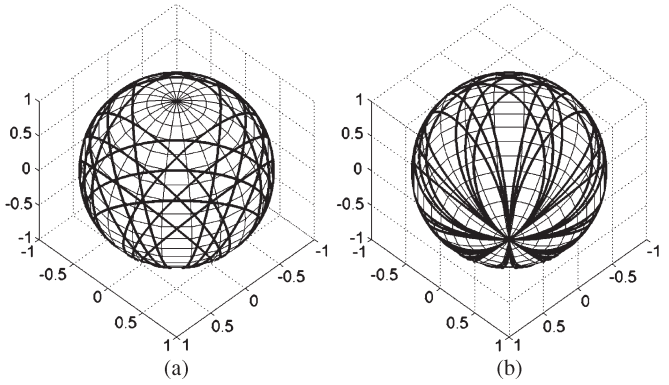

Fig. 1. Projection of the geodesic curves from (18) on $\mathbf{LIST}$ plotted on the gaze space $\mathbf{S}^2$. The left figure shows the north pole which is the frontal gaze direction. The right figure shows the south pole which is the backward gaze direction. The projections are circular passing through the backward gaze.

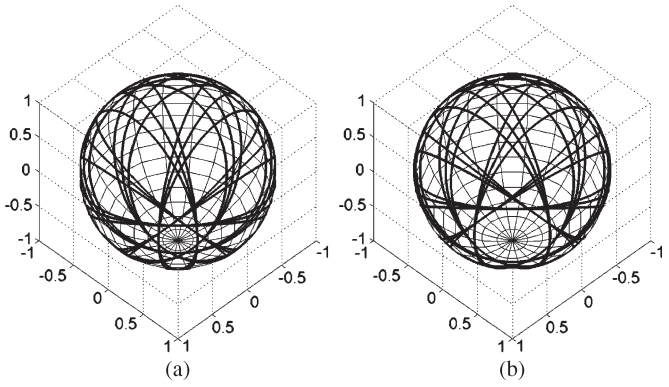

Fig. 2. Projection of the geodesic curves from (15) on $\mathbf{SO(3)}$ plotted on the gaze space $\mathbf{S}^2$. Both the left and the right figure show the south pole which is the backward gaze direction. As opposed to what we found in Fig. 1, each projection is a circle that do not pass through one fixed gaze and in particular through the backward gaze.

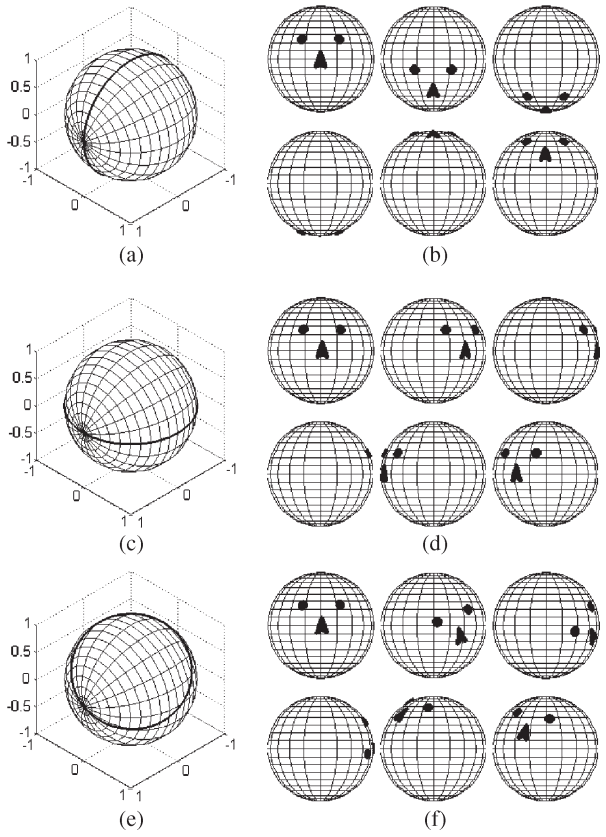

Fig. 3. Projection of the geodesic curves (16) on $\mathbf{DOND}$ plotted on the space $\mathbf{S}^2$ of pointing directions of the head. When the initial condition on $\dot{\theta}$ is zero, the axis of rotation does not change along the integral curves of (16) on $\mathbf{DOND}$. For different initial conditions on θ the pointing directions of the head rotate in a circle. (a) Head trajectory when $\theta = 0$. (b) For $\theta = 0$, head moves top to bottom without any torsion. (c) Head trajectory when $\theta = \pi/2$. (d) For $\theta = \pi/2$ head moves right to left without any torsion. (e) Head trajectory when $\theta = \pi/3$. (f) For $\theta = \pi/3$ head moves left/bottom to right/up with torsion.

VI. Some Simulations on Geodesic and Control Using Potential Function

In this section, our first goal is to show, using simulation, the shape of the geodesic trajectories on $\mathbf{SO}_L(3)$, $\mathbf{SO(3)}$ and $\mathbf{SO}_D(3)$. To display the shape, we plot the projection of the trajectories on $\mathbf{S}^2$.

A. Geodesic Trajectories

Example 1.1 (Geodesic Curves for Eye Movement Satisfying Listing): In this example we solve (18) (corresponds to eye rotation that satisfy the Listing's constraint). In Fig. 1 we have plotted the eye directions as a function of time starting from one suitably chosen initial condition. In plotting the figure, we have chosen the convention that the identity rotation matrix corresponds to the frontal gaze. Our simulation shows that the projection of the geodesic curve on the gaze space $\mathbf{S}^2$ is a circle that always passes through the backward gaze direction.

Example 1.2 (Geodesic Curves for Eye Movement Not Satisfying Listing): In this example we solve (15) (corresponds to eye rotation that does not satisfy the Listing's constraint). We show in Fig. 2 that the projection of the geodesic curves on the gaze space are circles that do not necessarily pass through a fixed point. Fig. 2(a) and (b) are two cases of the simulation assuming different initial conditions for $\dot{\alpha}$. Each figure consists of curves with different initial choices of θ and ϕ.

Remark: We have seen in Theorem 2 of Section III, that the geodesics on $\mathbf{SO}_L(3)$ and $\mathbf{SO(3)}$ are projections of great circles on $\mathbf{S}^3$. Their projections on the gaze space $\mathbf{S}^2$ are also circles that are plotted in Figs. 1 and 2.

Example 1.3 (Geodesic Curves for Head Movement Satisfying Donders): In this example, we solve (16) (corresponds to head rotation that satisfy the Donders' constraint). We assume that the initial condition on $\dot{\theta}$ is 0. In Fig. 3, we have plotted the pointing directions of the head as a function of time, starting from one suitably chosen initial head position, *viz.* "pointing straight with no tilt." The plot in Fig. 3 is shown for three different initial conditions on θ. The trajectories obtained in Fig. 3 are circles passing through the frontal pointing direction. For initial conditions on θ equals 0 or $\pi/2$, the axis of rotation is on the Listing's plane and the head rotates without any torsion, shown in Fig. 3(a)–(d). For other initial conditions, *viz.* $\theta = \pi/3$, the axis has torsional component provided by the Donder's Law (8), shown in Fig. 3(e) and (f). In this simulation, ϵ is chosen as 0.5.

Our next goal is to show that by tuning the parameters ϕ_0 and θ_0 in (21), we can drive the eye or the head to a suitable end position and orientation. This has been illustrated in the next three examples.

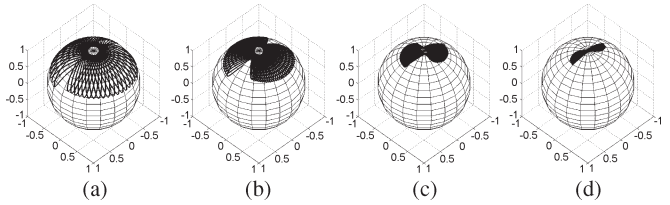

Fig. 4. Gaze motion from (25) for increasing values of the parameter A, with the external control set to zero, i.e., $\tau_\theta = \tau_\phi = 0$, and the motion is purely due to the potential function (21), which has a minimum at the frontal gaze. (a) $\mathrm{A} = 0.5$. (b) $\mathrm{A} = 1$. (c) $\mathrm{A} = 5$. (d) $\mathrm{A} = 50$.

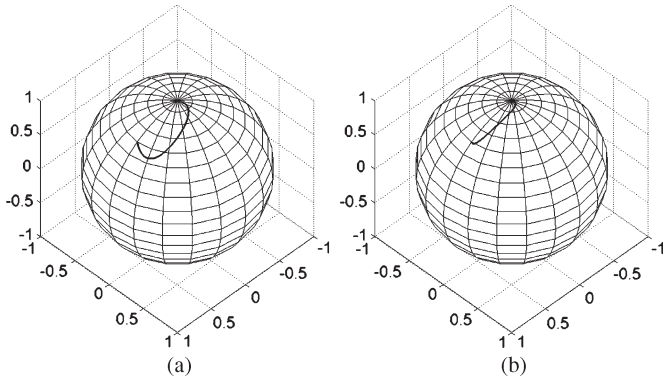

Fig. 5. Gaze motion under the influence of a potential function and a constant damping term using (25) with $\tau_\theta = -k\dot{\theta}$ and $\tau_\phi = -k\dot{\phi}$. The value of k is chosen to be 0.1. (a) $\mathrm{A} = 5$. (b) $\mathrm{A} = 50$.

B. Eye/Head Trajectories With a Potential Function

The purpose of this subsection is to demonstrate via simulation that by adding a potential term, one is able to push the trajectories of the eye or head toward the frontal gaze direction.

Example 2.1 (Eye Motion With a Potential Function But No Damping): In this example we solve (25) on **LIST** and display the gaze trajectories in Fig. 4. We have assumed $\tau_\theta = \tau_\phi = 0$, $\theta_0 = \phi_0 = 0$ and $B = 0$ in (21). Increasing magnitudes of A has been chosen in Fig. 4(a)–(d). Our simulations show that with increasing magnitude of the potential function, the gaze trajectories are restricted to a smaller neighborhood of the frontal gaze. However, the trajectories are oscillatory.

We now proceed to add a damping term to the motion equations.

Example 2.2 (Eye Regulation Toward Frontal Gaze Direction Using a Potential Function and Damping): We repeat Example 2.1 but choose $\tau_\theta = -.1\dot{\theta}$ and $\tau_\phi = -.1\dot{\phi}$ in (25), in order to dampen the fluctuations in the trajectories. The results are plotted in Fig. 5. We observe that the state settles down to the point of minimum potential, the frontal gaze.

Remark: Eye and head movements are damped in real system, through the actuating muscles. While modeling muscles, such as in [27] (see also [28]), a passive damping term is added to the model, which in turn damps the movement. In this paper we have not modeled damping of the real system, but introduced a damping term to study the effect of damping on the trajectories.

Example 2.3 (Head Regulation Toward an Arbitrary Heading Direction With Two Distinct Orientations): In this example, we have two head trajectories going to the same pointing direction but with two distinct orientations while satisfying the

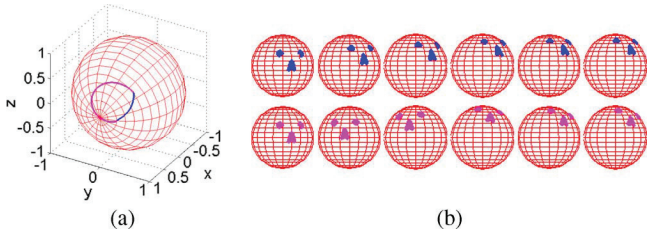

Fig. 6. Trajectories of the pointing directions with same initial head orientation and final head pointing direction. However, the final head orientations for the two trajectories are different. (a) Two trajectories of head movement from A to B. (b) Head orientations are shown for two trajectories. The top sequence is for the bottom trajectory in Fig. 6(a). The bottom sequence is for the top trajectory in Fig. 6(a).

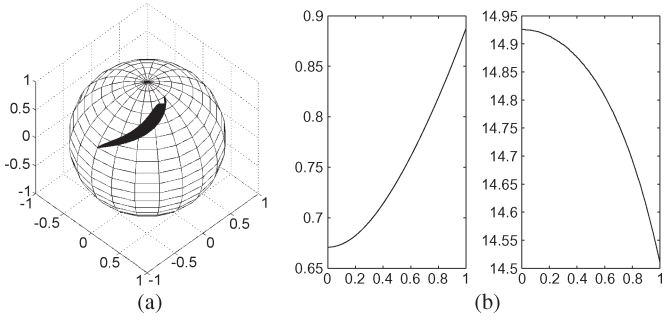

Fig. 7. For increasing values of ϵ, the head moves a longer distance in a shorter time. (a) Trajectories of the head direction as ϵ varies from 0 to 1. (b) (Left) distance as a function of ϵ. (Right) Time as a function of ϵ.

Donders' constraint. Possibility of two orientations for a given pointing direction is prescribed by the Donders' Theorem 3 in Appendix I. We have used the potential function (21) with $A = B = 1$ and $\tau_\theta = -1\dot{\theta}$ and $\tau_\phi = -1\dot{\phi}$. The parameters $\theta_0 = 5.5528$, $\phi_0 = -0.8026$ is chosen for the top trajectory in Fig. 6(a) and $\theta_0 = 2.3012$, $\phi_0 = 0.8026$ is chosen for the bottom trajectory in Fig. 6(a). The value of ϵ for the Donders' constraint is chosen as -0.1309. Fig. 6(b) show the head direction trajectories for the two paths. Fig. 6(b) shows the actual head orientations at initial, final and some intermediate points.

C. Effect of Donders' Torsional Component on Head Movement

Example 3 (How Does the Parameter ϵ Affect TIME and DISTANCE?): In Fig. 7, we have sketched the head movements between two specific directions, that are kept fixed for this example. In Fig. 7(a), head movements are shown for different values of ϵ in the Donders' constraint (8). The values of A, B in (21) are chosen to be 1. We choose $\tau_\theta = -1\dot{\theta}$ and $\tau_\phi = -1\dot{\phi}$. Although the paths appear to follow similar profile, in Fig. 7(b), we show that the total distance, computed using the Riemannian metric (14), increases with increasing values of ϵ. This is understandable since there is an extra head rotation for the same head direction. We also make a surprising observation in Fig. 7(b) that the time to complete the trajectories fall, as a function of ϵ, indicating that perhaps *with higher levels of torsion, provided by increasing ϵ, the head is able to move rapidly a larger distance in a shorter time*.

VII. Conclusion

In this paper, we study the problem of modeling the rotation of human head, when the head shifts its orientation between two pointing directions, as a simple mechanical system. The human eye is a special case of this class of problem. Head movements obey Donders' constraint (a generalization of the Listing's constraint for eye movement), which states that the allowed orientations of the head are obtained by rotating a fixed "primary heading direction" by a subclass of rotation matrices. These rotation matrices have their axes of rotation restricted to a fixed surface, called the Donders' surface. Defining a suitable Riemannian metric, we obtain dynamic model of head movement when the head orientations satisfy the Donders' constraint throughout its entire trajectory. Head movements are actuated by choosing a suitable potential function and the oscillations are damped by adding a suitable damping term. A similar study for the eye movement is reported in this paper assuming that the eye moves while Listing's constraint is always satisfied. For the head movement, an important result of this paper is to show the effect of the torsional component ϵ as head is allowed to move between two "pointing directions."

Among somewhat more theoretical results, we generalize the well known Listing's Theorem 1 which states that for all gaze directions, "other than one specific backward gaze," the orientation of the eye is a fixed function of gaze. For the head movement problem, a corresponding Donders' Theorem has been stated and proved in Appendix I. The Donders' theorem states that for all pointing directions of the head "other than a closed and bounded region $\mathbf{S}$" that contains the backward head direction, the orientation of the head for a specific "head direction" is ambiguous up to two alternative orientations (shown in Appendix I). Additionally—"within the closed and bounded region $\mathbf{S}$, the orientations of the head for a specific gaze direction is not unique but can have up to four distinct choices." A sketch of the set $\mathbf{S}$ for different values of ϵ has been shown in Fig. 9. Finally, in Appendix II, we obtain a suitable generalization of the half angle rule for head movement satisfying the Donders' constraint.

Research presented in this paper can be extended along the following three areas. Alternative forms of the potential function (22), chosen somewhat arbitrarily in this paper, can be explored to match recorded data from eye/head movement trajectories. Using τ_θ and τ_ϕ as the control variables for the dynamical system (25) describing head movements, one can solve minimum energy and minimum time optimal control problems. Finally, the same dynamical system (25) can also be used to study tracking problems, especially to track trajectories of recorded eye and head movement data.

Appendix I
Donders' Theorem

The question we ask in this appendix is the following:

Given a specific head direction, how many orientations of the head are allowed while satisfying the Donders' constraint? Equivalently, **For the map** (11), **how many pre-images does "proj" have?**

We now discuss this question as follows:

For a specific pointing direction $(a,b,c)^T$, where $a^2+b^2+c^2=1$, what are the possible values of θ and ϕ that will solve the set of equations

$$\begin{aligned}\sin\theta\sin\phi\cos\alpha+\cos\theta\sin^2\frac{\phi}{2}\sin 2\alpha&=a,\\ -\cos\theta\sin\phi\cos\alpha+\sin\theta\sin^2\frac{\phi}{2}\sin 2\alpha&=b,\\ \cos^2\frac{\phi}{2}-\sin^2\frac{\phi}{2}\cos 2\alpha&=c?\end{aligned}\tag{26}$$

(Generic Case When $\alpha\neq 0$ and $c\neq 1$): Multiplying the first equation by $\cos\theta$ and the second equation by $\sin\theta$ in (26), we obtain the following pair of equations:

$$\begin{aligned}\sin^2\frac{\phi}{2}\sin 2\alpha&=a\cos\theta+b\sin\theta,\\ \cos^2\frac{\phi}{2}-\sin^2\frac{\phi}{2}\cos 2\alpha&=c.\end{aligned}\tag{27}$$

From (27) we obtain the following:

$$\begin{aligned}\sin^2\frac{\phi}{2}&=\frac{a\cos\theta+b\sin\theta}{\sin 2\alpha},\\ \cos^2\frac{\phi}{2}&=\frac{c\sin 2\alpha+(a\cos\theta+b\sin\theta)\cos 2\alpha}{\sin 2\alpha}.\end{aligned}\tag{28}$$

Eliminating ϕ from (28), we obtain

$$\frac{a}{1-c}\cos\theta+\frac{b}{1-c}\sin\theta=\frac{\sin 2\alpha}{1+\cos 2\alpha}\tag{29}$$

where α is given by (8), and ϵ is assumed small enough such that $\alpha\neq\pi$. If θ_0 is the angle the vector $(a,b)^T$ makes with respect to the positive x-axis, we can rewrite (29) as

$$\sqrt{\frac{1+c}{1-c}}\cos(\theta-\theta_0)=\frac{\sin 2\alpha}{1+\cos 2\alpha}.\tag{30}$$

We solve (30) by plotting the right-hand side in red and the left-hand side in blue as has been shown in Fig. 8. The x-coordinate is the θ-axis. The points of intersections are the values of θ that solve (30). We have chosen $\epsilon=0.5$, $a=r\cos\gamma$, $b=+r\sin\gamma$, and $c=\pm\sqrt{1-(a^2+b^2)}$. The parameter r is varied from 0.1 to 0.9. In the top three subfigures of Fig. 8, the parameter c is chosen to be negative, i.e., the head direction is in the backward hemisphere; for smaller values of r (curves with smaller amplitude) there are four points of intersections; for larger values of r (curves with larger amplitude) there are two points of intersections. In the bottom three figures of Fig. 8, the parameter c is chosen to be positive, i.e., the head direction is in the frontal hemisphere; for every value of r, the number of intersection points is two. For each possible choice of θ, we can use (28) to calculate the rotation angle ϕ.

Theorem 3 (Donders): For a specific pointing direction, (30) can be solved for θ up to 2 or 4 alternative solutions, counting multiplicities. Hence, the number of orientations for a given pointing directions of the head is either 2 or 4 counting multiplicities.

Proof of Theorem 3: The generic case when $\alpha\neq 0$ and $c\neq 1$, has already been discussed before. The non generic special cases are discussed below:

(Special Case When $\alpha=0$): In this case, θ is either 0, $\pi/2$, π or $3\pi/2$. When $\theta=0$, we have $a=0$, $b=-\sin\phi$ and $c=$

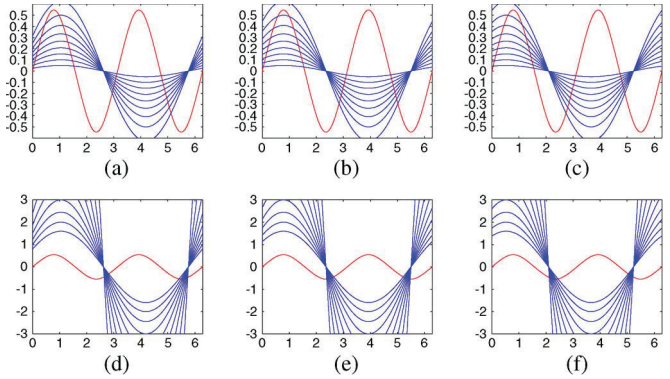

Fig. 8. In this figure we show that θ can be solved up to two or four alternative choices. (a) Back Hemisphere along $\gamma = \pi/3$. (b) Back Hemisphere along $\gamma = \pi/4$. (c) Back Hemisphere along $\gamma = \pi/6$. (d) Front Hemisphere along $\gamma = \pi/3$. (e) Front Hemisphere along $\gamma = \pi/4$. (f) Front Hemisphere along $\gamma = \pi/6$.

$\cos\phi$; when $\theta = \pi$, we have $a = 0$, $b = \sin\phi$ and $c = \cos\phi$. Finally, when $\theta = \pi/2$ we have $b = 0$, $a = \sin\phi$ and $c = \cos\phi$ and when $\theta = 3\pi/2$ we have $b = 0$, $a = -\sin\phi$ and $c = \cos\phi$. The rotation matrix (1) is uniquely given by

$$\begin{pmatrix} 1 & 0 & 0 \\ 0 & c & b \\ 0 & -b & c \end{pmatrix}, \quad \text{when } \theta = 0 \text{ or } \pi \tag{31}$$

and

$$\begin{pmatrix} c & 0 & a \\ 0 & 1 & 0 \\ -a & 0 & c \end{pmatrix}, \quad \text{when } \theta = \frac{\pi}{2} \text{ or } \frac{3\pi}{2}. \tag{32}$$

From (31) we infer that when $a = b = 0$ and $c = -1$, the gaze direction is precisely backwards. There are exactly two distinct preimages of the mapping "proj" given by

$$\begin{pmatrix} 1 & 0 & 0 \\ 0 & -1 & 0 \\ 0 & 0 & -1 \end{pmatrix} \quad \text{and} \quad \begin{pmatrix} -1 & 0 & 0 \\ 0 & 1 & 0 \\ 0 & 0 & -1 \end{pmatrix}. \tag{33}$$

(Special Case When $c = 1$): In this case, it would follow that $a = b = 0$. From (27) we would infer that

$$\sin^2\frac{\phi}{2}\sin 2\alpha = 0;\ \cos^2\frac{\phi}{2} - \sin^2\frac{\phi}{2}\cos 2\alpha = 1. \tag{34}$$

We deduce from (34) that $\phi = 0$ and θ is arbitrary. The rotation matrix W, given by (1), is trivially the identity matrix.$(\mathbf{Q.E.D})$

The main result of Appendix I can be summarized as follows: For head rotation satisfying Donders' Law, for a specific head direction, the head orientation matrix is not necessarily unique but can be ambiguous up to two or four choices. If ϵ is chosen to be 0.5, we observe graphically in Fig. 8(d)–(f) that for head direction in the front hemisphere, the head orientation is unique up to two choices. For head direction in the back hemisphere, the head orientation is ambiguous up to two choices, until a threshold, as evidenced by Fig. 8(a)–(c). Closer to the backward head direction, the number of possible head orientations, for a specific head direction, splits up to four. This is also evident in Figs. 8(a)–(c) where we notice that blue curves of lower amplitude intersect the red curve at four distinct points.

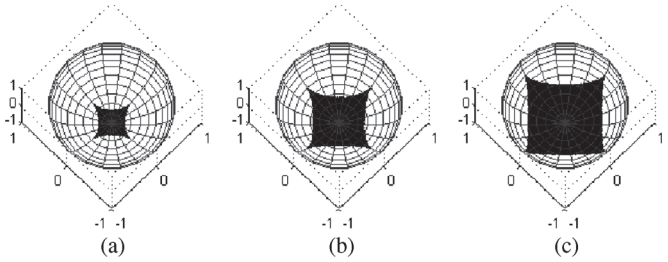

Fig. 9. Backward pointing direction of the head is shown as the south pole. The shaded regions $\mathbf{S}$ around the south pole has been sketched for different values of ϵ. (a) $\epsilon = 0.1$. (b) $\epsilon = 0.2$. (c) $\epsilon = 0.3$.

For different values of ϵ in the Donders' constraint (8), the threshold has been computed where the number of solutions of (30) jump from 2 to 4, and has been sketched in Fig. 9. Outside the shaded region $\mathbf{S}$ in Fig. 9, the number of solutions of (30) is precisely 2, counting multiplicity. Inside the shaded region $\mathbf{S}$ in Fig. 9, the number of solutions of (30) is no more than 4, and is precisely 4 almost everywhere.

Example I.1 (Example Indicating Two Alternative Solutions Under Donders' Law: In this example we consider Donders' constraint (8) by selecting $\epsilon = 0.5$. For a specific head direction vector $(0.4330\ -0.2500\ 0.8660)$, we solve (30) and obtain $\theta = .9053$ and $\theta = 4.2934$ to be the two distinct solutions. The corresponding values of ϕ are given by $\phi = .5940$ and $\theta = -.5630$. The corresponding orthogonal matrices (1) are given by

$$\begin{pmatrix} +0.8798 & -0.1962 & +0.4330 \\ +0.3264 & +0.9116 & -0.2500 \\ -0.3457 & +0.3613 & +0.8660 \end{pmatrix}$$

$$\text{and} \quad \begin{pmatrix} +0.8678 & +0.2436 & +0.4330 \\ -0.1440 & +0.9575 & -0.2500 \\ -0.4755 & +0.1546 & +0.8660 \end{pmatrix}. \tag{35}$$

Note that the last column of the above two matrices are the same indicating the pointing direction. The first two columns are the orientations of the head. The example shows two distinct orientations for the same head direction. Pointing directions for which the number of distinct solutions of θ is 4 has not been considered in this example.

Example I.2 (Potential Control That Transfers Between Two Orientations of the Head at a Given Fixed Pointing Direction): In this example, we construct trajectories on the space $\mathbf{S}^2$ of pointing directions of the head that start and end at the same point. However, the initial and the final point do not correspond to the same orientation of the head. The trajectories are constructed using the potential function (21) assuming $A = B = 1.0$, together with a suitable damping control $\tau_\theta = -1\dot{\theta}$ and $\tau_\phi = -1\dot{\phi}$. Starting from a fixed pointing direction, two trajectories have been constructed that start and end at the two corresponding head orientations. The results have been displayed in Fig. 10. In Fig. 10(a) the blue trajectory is clockwise from left to right as shown in Fig. 10(b). Correspondingly the black trajectory is anti clockwise from left to right. The extreme left and right orientations correspond to the same pointing direction of the head. In this simulation, ϵ has been chosen as -0.1309.

Remark: One can conclude from the simulation result displayed in Fig. 10 that if Donders' constraint has to be satisfied

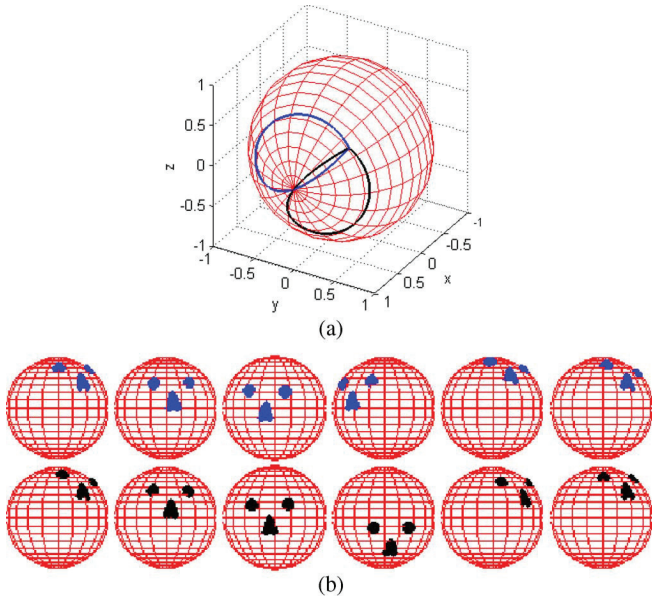

Fig. 10. Orientation flipping head movement using potential control and satisfying Donders' constraint. (a) Two trajectories on the space $\mathbf{S}^2$ of pointing directions of the head. (b) Each of the two trajectories are displayed from left to right showing the head orientations.

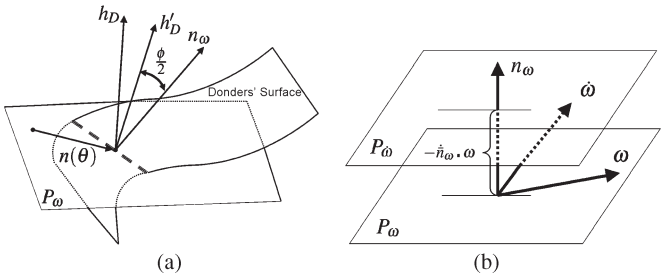

Fig. 11. Figure illustrates the construction of P_ω and $P_{\dot\omega}$. (a) Plane P_ω containing the angular velocity vectors. (b) Planes P_ω and $P_{\dot\omega}$ are parallel.

throughout the trajectory of head movement, "orientation flipping" would require the head to move along a cycle. It is unclear, if such "head movement gaits" have any functional significance.

Appendix II
Half Angle Rule

Starting from a specific orientation, in order for the head to move satisfying the Donders' constraint (8), the angular velocity and acceleration vectors have to satisfy a constraint. In fact, these vectors have to lie in a plane that changes with the moving head. The "half angle rule," we consider in this appendix, describes this moving plane. For the eye movement problem satisfying Listing's law such a half angle rule is already known (see [21]). We obtain a generalization of the half angle rule that would apply to the head movement problem satisfying Donders' constraint. Clearly, half angle rule would be an important constraint to be satisfied in order for the head orientations to satisfy Donders' constraint.

Let us rewrite the unit quaternion (2) as

$$q(t) = \begin{pmatrix} \cos\frac{\phi(t)}{2} \\ \sin\frac{\phi(t)}{2} n(t) \end{pmatrix} \tag{36}$$

where $n(t)$ is the axis of rotation given by (9). The time derivative of q can be expressed as (see [29])

$$\dot q(t) = \frac{1}{2}\tilde\omega(t) \bullet q(t) \tag{37}$$

where $\tilde\omega = (0, \omega)$ is a quaternion whose vector part ω is the angular velocity of the "head" with respect to a fixed universal coordinate attached to the "body." (In case of eye movement, ω is the angular velocity of the "eye" with respect to a coordinate fixed to the "head.") The formula (37) can be rewritten as

$$\dot q(t) = \frac{1}{2}\begin{pmatrix} -(\omega \cdot n)\sin\frac{\phi}{2} \\ \omega\cos\frac{\phi}{2} + (\omega \times n)\sin\frac{\phi}{2} \end{pmatrix}. \tag{38}$$

By computing the derivative of (36), we obtain

$$\dot q(t) = \frac{1}{2}\begin{pmatrix} -\sin\frac{\phi}{2}\dot\phi \\ 2\sin\frac{\phi}{2}\dot n + \cos\frac{\phi}{2}\dot\phi n \end{pmatrix}. \tag{39}$$

Comparing (38) and (39) we obtain

$$\dot\phi = \omega \cdot n \tag{40}$$

and

$$\sin\frac{\phi}{2}\dot n = \frac{1}{2}\cos\frac{\phi}{2}\omega + \frac{1}{2}\sin\frac{\phi}{2}(\omega \times n) - \left(\frac{1}{2}\cos\frac{\phi}{2}\dot\phi\right) n. \tag{41}$$

Let h_D be a vector perpendicular to the Donders' surface at θ. We have

$$\begin{aligned} h_D \cdot \dot n = 0 \Rightarrow\ & (h_D \cdot \omega)\cos\frac{\phi}{2} + h_D \cdot (\omega \times n)\sin\frac{\phi}{2} \\ & - (\omega \cdot n)(h_D \cdot n)\cos\frac{\phi}{2} \\ = 0 \Rightarrow\ & \left(h_D\cos\frac{\phi}{2} - (h_D \times n)\sin\frac{\phi}{2} - (h_D \cdot n)\cos\frac{\phi}{2} n\right) \cdot \omega \\ = 0. & \end{aligned} \tag{42}$$

Writing

$$h'_D = h_D - (h_D \cdot n)n$$

we obtain

$$\left(h'_D\cos\frac{\phi}{2} - (h'_D \times n)\sin\frac{\phi}{2}\right) \cdot \omega = 0. \tag{43}$$

Note that h'_D is an orthogonalization of h_D with respect to the unit "axis of rotation" vector n. It follows from (43) that:

> The angular velocity vector must belong to a plane P_ω passing through n whose normal forms an angle $\phi/2$ with respect to the orthogonalized h'_D.

Remark: One way to think about generating the plane P_ω is to start from h_D and obtain h'_D by orthogonalization. Subsequently rotate using the right-hand rule the vector h'_D along the axis n by an angle $\phi/2$. The obtained vector n_ω is orthogonal to the plane P_ω (see Fig. 11(a) for an illustration).

Remark: For the case of eye movement satisfying Listing's Law, the vectors h_D and h'_D are the same vectors and they are

equal to $(0,0,1)^T$. It is straightforward to verify that the angular velocity vector $(\omega_1,\omega_2,\omega_3)^T$ is given by

$$\begin{pmatrix}\omega_1\\ \omega_2\\ \omega_3\end{pmatrix}=\begin{pmatrix}\cos\theta\\ \sin\theta\\ 0\end{pmatrix}\dot{\phi}+\begin{pmatrix}-\cos\frac{\phi}{2}\sin\theta\\ \cos\frac{\phi}{2}\cos\theta\\ \sin\frac{\phi}{2}\end{pmatrix}2\sin\frac{\phi}{2}\dot{\theta}.$$

So in the case of "Listing," the vector n_ω is explicitly given by

$$\left(\sin\theta\ \sin\frac{\phi}{2}\ -\cos\theta\ \sin\frac{\phi}{2}\ \cos\frac{\phi}{2}\right)^T$$

which clearly has an angle $\phi/2$ with respect to the vector $(0,0,1)^T$. We now state the following theorem.

Theorem 4 (Half Angle Rule): A necessary condition for the axis of rotation vector

$$n(\theta)=(\cos\theta\cos\alpha,\ \sin\theta\cos\alpha,\ \sin\alpha)^T,\ \alpha=\epsilon\sin(2\theta)$$

to remain inside the Donders' surface (10) is described as follows. For each value of θ, the angular velocity vector must be confined to a plane P_ω passing through n whose normal forms an angle $\phi/2$ with respect to the vector h'_D, where h'_D is the orthogonalization of h_D with respect to n. Finally, when $\phi\neq 0$ the above necessary condition is also sufficient.

Proof of Theorem 4: The necessity of the half angle rule has already been sketched in (41), (42), and (43). When $\phi\neq 0$, using (41), it would follow that the implications in (42) can be reversed. Thus, the half angle rule is also sufficient. $(\mathbf{Q.E.D})$

In closing this appendix, we would like to claim that in order for the Donders' constraint to be satisfied, the angular acceleration vector must be constrained to an affine plane parallel to P_ω. Let us define

$$\bar{n}_\omega=\frac{n_\omega}{||n_\omega||}$$

where we have $\bar{n}_\omega\cdot\omega=0$. It follows that the angular acceleration vector $\dot{\omega}$ satisfies $\bar{n}_\omega\cdot\dot{\omega}=-\dot{\bar{n}}_\omega\cdot\omega$. Note that $\bar{n}_\omega\cdot\dot{\omega}$ is the scalar projection of the vector $\dot{\omega}$ on the vector n_ω normal to the plane P_ω. The acceleration vectors are thus confined to a plane $P_{\dot{\omega}}$ with the property that its scalar projection on n_ω is given by $-\dot{\bar{n}}_\omega\cdot\omega$. It follows that the acceleration vectors lie in a plane $P_{\dot{\omega}}$ parallel to the plane P_ω at a distance $-\dot{\bar{n}}_\omega\cdot\omega$ (see Fig. 11(b) for an illustration).

We remark that the vector $\dot{\bar{n}}_\omega$ is perpendicular to n_ω and hence it belongs to the plane P_ω. Under the Listing's constraint, it has been shown in [21] that the vector $\dot{\bar{n}}_\omega$ is perpendicular to ω. It would therefore follow that for this case, P_ω and $P_{\dot{\omega}}$ are the same plane, as already claimed in [21].

ACKNOWLEDGMENT

A good part of this paper was completed when the first author was visiting the "Cognition for Technical Systems" cluster (CoTeSys) at the Technical University of Munich, Germany during May 2010. Hospitality of Profs. M. Buss and S. Hirche is gratefully acknowledged. Discussions with Dr. E. Schneider and Dr. S. Glasauer, from Ludwig Maximilians University, Munich, on various aspects of the eye and the head movement problem also helped in shaping this paper.

REFERENCES

[1] J. B. Listing, *Beiträge zur physiologischen optik*. Göttingen, Germany: Göttinger Studien, Vandenhoeck und Ruprecht, 1845.
[2] F. C. Donders, "Beiträge zur lehre von den bewegungen des menschlichen auges," *Holländische Beiträge zu den anatomischen und physiologischen Wissenschaften*, vol. 1, pp. 104–145, 1996, 1848. Press.
[3] H. von Helmholtz, *Handbuch der Physiologischen Optik.*, 3rd ed. Leipzig, Germany: Leopold Voss, Hamburg & Leipzig, 1910, vol. 1866, no. 3.
[4] W. P. Medendorp, J. A. M. V. Gisbergen, M. W. I. M. Horstink, and C. C. A. M. Gielen, "Donders' law torticollis," *J. Neurophysiology*, vol. 82, pp. 2833–2838, 1999.
[5] P. Radau, D. Tweed, and T. Vilis, "Three dimensional eye head and chest orientations following large gaze shifts and the underlying neural strategies," *J. Neurophysiol.*, vol. 72, pp. 2840–2852, 1994.
[6] D. Robinson, "The mechanics of human saccadic eye movement," *J. Physiol.*, vol. 174, pp. 245–264, 1964.
[7] D. Tweed, "Three dimensional model of the human eye-head saccadic system," *J. Neurophysiology*, vol. 77, pp. 654–666, 1997.
[8] D. Tweed and T. Villis, "Implications of rotational kinematics for the oculomotor system three dimensions," *J. Neurophysiol.*, vol. 58, no. 4, pp. 832–849, 1987.
[9] D. Tweed and T. Villis, "Geometric relations of eye position and velocity vectors during saccades," *Vis. Res.*, vol. 30, pp. 111–127, 1990.
[10] T. Haslwanter, "Mathematics of three-dimensional eye rotations," *Vision Res.*, vol. 35, no. 12, pp. 1727–1739, 1995.
[11] T. Haslwanter, "Mechanics of eye movements: Implications of the orbital revolution," *Ann. N. Y. Acad. Sci.*, vol. 956, pp. 33–41, 2002.
[12] D. Tweed, T. Haslwanter, and M. Fetter, "Optimizing gaze control three dimensions," *Science*, vol. 281, no. 28, pp. 1363–1365, Aug. 1998.
[13] A. A. Handzel and T. Flash, "The geometry of eye rotations and listing's law," *Adv. Neural Inf. Process. Syst.*, vol. 8, pp. 117–123, 1996.
[14] D. Angelaki and B. J. M. Hess, "Control of eye orientation: Where does the brain's role end and the muscle's beg (review article)," *Eur. J. Neurosci.*, vol. 19, pp. 1–10, 2004.
[15] S. Glasauer, "Current models of the ocular motor system," *Neuro-Ophthalmology, Dev. Ophthalmology*, vol. 40, pp. 158–174, 2007.
[16] J. D. Crawford, J. C. Martinez-Trujillo, and E. M. Klier, "Control of three-dimensional eye and head movements," *Current Opinion in Neurobiol.*, vol. 13, no. 6, pp. 655–662, Dec. 2003.
[17] R. Abraham and J. E. Marsden, *Foundations of Mechanics*. Providence, RI: AMS Chelsea Publishing, American Mathematical Society, 1978.
[18] F. Bullo and A. D. Lewis, *Geometric Control of Mechanical Systems*. Berlin, Germany: Springer-Verlag, 2004.
[19] R. M. Murray, "Nonlinear control of mechanical systems: A Lagrangian perspective," *Annu. Rev. Control*, vol. 21, pp. 31–45, 1997.
[20] A. D. Polpitiya, W. P. Dayawansa, C. F. Martin, and B. K. Ghosh, "Geometry and control of human eye movements," *IEEE Trans. Autom. Control*, vol. 52, no. 2, pp. 170–180, Feb. 2007.
[21] G. Cannata and M. Maggiali, "Models for the design of bioinspired robot eyes," *IEEE Trans. Robotics*, vol. 24, no. 1, pp. 27–44, Feb. 2008.
[22] W. M. Boothby, *An Introduction to Differentiable Manifolds and Riemannian Geometry*. San Diego, CA: Academic, 1986.
[23] B. K. Ghosh and I. B. Wijayasinghe, "Dynamic control of human eye on head system," in *Proc. 29th Chinese Control Conf.*, Beijing, China, Jul. 2010, pp. 5514–5519.
[24] S. L. Altmann, *Rotations, Quaternions, Double Groups*. Oxford, U.K.: Oxford Univ. Press (Hardcover), 1986, Dover (Paperback)., 2005.
[25] J. B. Kuipers, *Quaternions and Rotation Sequences*. Princeton, NJ: Princeton Univ. Press, 2002.
[26] H. Weyl, *The Concept of a Riemann Surface*. New York: Addison-Wesley Pub. Co. (Hardcover), 1964, Dover(Paperback), 2009.
[27] A. Hill, "The heat of shortening and dynamic constants of muscle," *Proc. R. Soc. B.*, vol. 126, pp. 136–195, 1938.
[28] F. Zajak, "Muscle and tendon: Properties, models, scaling and application to biomechanics and motor control," *CRC Critical Rev. Biomed. Eng.*, vol. 17, pp. 359–511, 1989.
[29] R. M. Murray, Z. Li, and S. S. Sastry, *A Mathematical Introduction to Robotic Manipulation*. Boca Raton, FL: CRC, 1994.

Bijoy K. Ghosh (F'00) received the B.Tech. and M.Tech. degrees in electrical and electronics engineering from BITS Pilani and the Indian Institute of Technology, Kanpur, India, and the Ph.D. degree in Engineering Sciences from the Decision and Control Group, Division of Applied Sciences, Harvard University, Cambridge, MA, in 1977, 1979 and 1983, respectively.

From 1983 to 2007, he was with the Department of Electrical and Systems Engineering, Washington University, St. Louis, MO, where he was a Professor and Director of the Center for BioCybernetics and Intelligent Systems. Currently, he is the Dick and Martha Brooks Regents Professor of Mathematics and Statistics at Texas Tech University, Lubbock. He had held visiting positions at the Tokyo Institute of Technology and Tokyo Denki University, Japan, University of Padova in Italy, Royal Institute of Technology and Institut Mittag-Leffler, Stockholm, Sweden, Yale University, New Haven, CT, Technical University of Munich, Germany, and Indian Institute of Technology, Kharagpur, India. His research interests are in Control Theory, Bio Systems and Control and Bio Informatics.

Prof. Ghosh received the Donald P. Eckmann award in 1988 from the American Automatic Control Council and the Japan Society for the Promotion of Sciences Invitation Fellowship in 1997. He is the IEEE Control Systems Society Representative to the IEEE-USA's Medical Technology Policy Committee and a member of the Editorial Board of the IEEE TRANSACTIONS ON COMPUTATIONAL BIOLOGY AND BIOINFORMATICS.

Indika B. Wijayasinghe (M'09) received the B.Sc. degree in electrical and electronics engineering from University of Peradeniya, Peradeniya, Sri Lanka, in 2007. He is currently pursuing the Ph.D. degree in the Center for BioCybernetics and Intelligent Systems, Department of Mathematics and Statistics, Texas Tech University, Lubbock.

His research interests are in control theory and bio mechanics.